13th International Symposium on Turbulence and Shear Flow Phenomena (TSFP13)
Montreal, Canada, June 25-28, 2024

A GNN-BASED COMPREHENSIVE SGS STRESS MODEL FOR TURBULENCE AND TURBULENT COMBUSTION

Haruya Shimamoto
Department of Mechanical Engineering
Tokyo Institute of Technology
2-12-1 Ookayama, Meguro-ku,
Tokyo 152-8550, Japan
shimamoto.h.ac@m.titech.ac.jp

Ye Wang
Department of Mechanical Engineering
Tokyo Institute of Technology
2-12-1 Ookayama, Meguro-ku,
Tokyo 152-8550, Japan
wang.y.by@m.titech.ac.jp

Sayaka Suzuki
Department of Mechanical Engineering
Tokyo Institute of Technology
2-12-1 Ookayama, Meguro-ku,
Tokyo 152-8550, Japan
suzuki.s.dq@m.titech.ac.jp

Mamoru Tanahashi
Department of Mechanical Engineering
Tokyo Institute of Technology
2-12-1 Ookayama, Meguro-ku,
Tokyo 152-8550, Japan
tanahashi.m.aa@m.titech.ac.jp

ABSTRACT

Machine learning (ML) techniques have been employed in subgrid scale (SGS) stress modeling in the context of large eddy simulation (LES) recently. However, many of the current ML-based models include limitations associated with practical applications, such as incompatibility with unstructured meshes and limited applicability of the model. In the present study, a graph neural network (GNN) is employed to overcome those limitations while achieving high prediction performance by considering the adjacent features through convolution. Direct numerical simulation (DNS) data of various types of turbulent flow fields are used in the process of training, validation, and testing of the model. The GNN-based SGS stress model is assessed in a priori manner in both non-reacting incompressible turbulent flows and reacting combustion fields. The result of a priori testing in incompressible turbulent flows shows that the correlation coefficient surpasses 0.8 in all test cases. Furthermore, the model exhibits good agreement with the filtered DNS of variable-density turbulent combustion fields within the reaction zones, although the errors are slightly larger in the diagonal components due to dilation. Future work includes the improvement of prediction performance in regions with large density fluctuations by incorporating turbulent combustion fields in the training dataset.

INTRODUCTION

With the increase in computational capabilities, LES is becoming a valid tool for fluid equipment design. LES requires less computational costs compared with DNS due to resolving only grid-scale (GS) components, while the contributions from subgrid-scale (SGS) ones are modeled by the SGS stress model. In recent years, machine learning has been employed in wide range of fields such as image recognition (Krizhevsky *et al*., 2012) and language processing (Sutskever *et al.*, 2014), and SGS stress modeling is no exception. Reportedly ML-based models outperform conventional models in terms of a priori testing (Nikolaou *et al.*, 2020; Liu *et al*., 2022). However, the ML-based modeling approach has the following potential limitations when it comes to practical applications: feature sampling incompatible near the physical boundary regions and for non-uniform meshes, and models trained specific to single flow configuration. For example, convolutional neural network (CNN) postulates uniform Cartesian mesh in feature sampling, which may not be always applicable to complex meshes such as unstructured mesh or non-uniform mesh. Moreover, a part of the CNN kernel subdomain could be outside the flow area near the physical boundaries. ML-based models trained on single flow configuration may be significantly less accurate in other flow configurations or the flow configuration that is physically identical to the one from which the model is trained but translated or rotated due to lack of physical invariants.

In the present study, the SGS stress model is developed based on GNN to resolve above-mentioned limitations in the context of LES using DNS data as training dataset. In creating training dataset, data augmentation is applied to satisfy the rotational invariant. First, a priori assessment is performed for a range of turbulent flow configurations. Subsequently, the prediction performance of the developed model is further tested in two different types of variable-density turbulent combustion fields in a priori manner. The details of the neural network architecture, input/output quantities, and training dataset are introduced in the next section, followed by the results of the model assessment and discussion.

SGS STRESS MODELING

The SGS stress tensor appearing in the filtered Navier-Stokes equation needs to be modeled:

$$\tau_{ij} = \bar{\rho}(\widetilde{u_i u_j} - \tilde{u}_i \tilde{u}_j), \tag{1}$$

where the overline and the tilde denote spatial filtering and

Favre filtering, respectively. Here, compressible flows are considered in the SGS stress tensor for generality since reacting flow conditions are also considered as later described. In the present study, the SGS stress model is developed based on graph neural network (GNN). GNN is a type of deep neural network architectures suited for data structured as graphs. A graph consists of nodes and edges, and the computational mesh on which the flow field is discretized can be regarded as a graph data in the context of computational fluid dynamics. Therefore, GNN does not require uniform Cartesian mesh as input/output quantities.

The spatial convolutional GNN based on SplineCNN (Fey *et al.*, 2018) is employed as the neural network architecture, which takes into account the relative positions of the adjacent nodes by the edge feature constructed as

$$e(i,j) = \frac{1}{N_e \Delta}(x_i - x_j, y_i - y_j, z_i - z_j) + \frac{1}{2}, \qquad (2)$$

where N_e is the normalizing factor to satisfy $\|e\| \leq 1$, and Δ is the filter size considered in the model. A total of thirteen quantities adopted in the previous study (Abekawa *et al.*, 2023) are fed into the input layer,

$$\partial \tilde{u}_i / \partial x_j, \qquad (3)$$

$$\exp(-d_{\mathrm{wall}}/\Delta), \qquad (4)$$

$$\tilde{u}_i - \langle \tilde{u}_i \rangle_\Delta, \qquad (5)$$

where $\langle \cdot \rangle_\Delta$ denotes the mean value at the reference point and its adjacent points. The output quantities are six SGS stress tensor components. Among the inputs, the velocity gradient is typically used in traditional SGS models such as the Smagorinsky model (Smagorinsky, 1963) and the gradient model (Clark, 1979; Vreman *et al.*, 1996). It was shown that the wall distance d_{wall} improves the model performance for turbulent channel flow (Gamahara and Hattori, 2017). However, the direct incorporation of the wall distance into the model causes a feature scaling issue. Eq. (4) is introduced so that the value ranges between 0 and 1 for $0 \leq d_{\mathrm{wall}} < \infty$. Eq. (5) mimics the velocity fluctuation used in scale-similarity model (Bardina, 1983).

The neural network structure is shown in Figure 1. The input layer is followed by two SplineCNN layers, whose outputs are aggregated by the scatter mean layer. Subsequently, two fully-connected (dense) layers precede the final output layer. The SplineCNN layers are denoted as $\mathrm{SConv}(k, M_{in}, M_{out})$, where $k = (k_1, k_2, k_3)$ is the multi-dimensional kernel size, M_{in} is the size of the input feature map, and M_{out} is the size of the output feature map. The details of the GNN architecture are as follows. The degree of the B-spline basis b_m is taken as 1 based on the parametric study in Fey *et al.*, and $k_1 = k_2 = k_3 = b_m + 4$ for Cartesian coordinate. The aggregation in the GNN layers is achieved by calculating the mean value of the corresponding graph nodes. Thus, the performance of the model is not substantially influenced by the variations in the number of adjacent points. As activation functions, the exponential liner unit (ELU) activation function is employed except for the second fully-connected layer, where the rectified linear unit (ReLU) activation function is employed. In addition, ReLU function is applied only to the diagonal components of the six output tensor components after the last fully-connected layer to enforce general $\tau_{ii} > 0$ constraint.

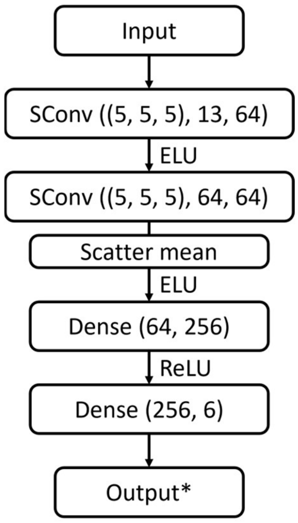

Figure 1. The structure of the GNN model. Note that the ReLU function is additionally applied to the diagonal components at the output layer.

Incompressible DNS results of homogeneous isotropic turbulence (HIT) (Tanahashi *et al.*, 1999), turbulent channel flow (CH) (Tanahashi *et al.*, 2004; Kang *et al.*, 2007) and temporally developing turbulent mixing layer (TML) (Tanahashi *et al.*, 2001; Itoh *et al.*, 2018) are used in the process of training and testing of the GNN model. These turbulent flow fields are shown in Figure 2 in terms of the isosurface of the second invariant of the velocity gradient tensor. The numerical conditions of the DNS data are summarized in Table 1, where Reynolds number is based on Taylor microscale for HIT, friction velocity for CH and the

Table 1. Numerical conditions of the DNS dataset

Flow	*Re*	$L_x \times L_y \times L_z$	$N_x \times N_y \times N_z$
HIT	60	$2\pi \times 2\pi \times 2\pi$	128^3
	97	$2\pi \times 2\pi \times 2\pi$	256^3
	120	$2\pi \times 2\pi \times 2\pi$	324^3
	141	$2\pi \times 2\pi \times 2\pi$	400^3
CH	180	$4\pi\delta \times 2\delta \times \pi\delta$	$192 \times 193 \times 160$
	400	$2\pi\delta \times 2\delta \times \pi\delta$	$256 \times 385 \times 192$
	800	$2\pi\delta \times 2\delta \times \pi\delta$	$512 \times 769 \times 384$
	1295	$2\pi\delta \times 2\delta \times \pi\delta$	$864 \times 1239 \times 648$
TML	500	$4\Lambda \times 6\Lambda \times 8/3\Lambda$	$216 \times 325 \times 144$
	1100	$4\Lambda \times 6\Lambda \times 8/3\Lambda$	$360 \times 541 \times 240$
	1300	$4\Lambda \times 6\Lambda \times 8/3\Lambda$	$384 \times 577 \times 240$
	1900	$4\Lambda \times 6\Lambda \times 8/3\Lambda$	$480 \times 721 \times 320$
PF	60	$5 \times 2.5 \times 2.5\ \mathrm{mm}^3$	$513 \times 128 \times 128$
VF	97	$10 \times 5 \times 5\ \mathrm{mm}^3$	$769 \times 385 \times 385$

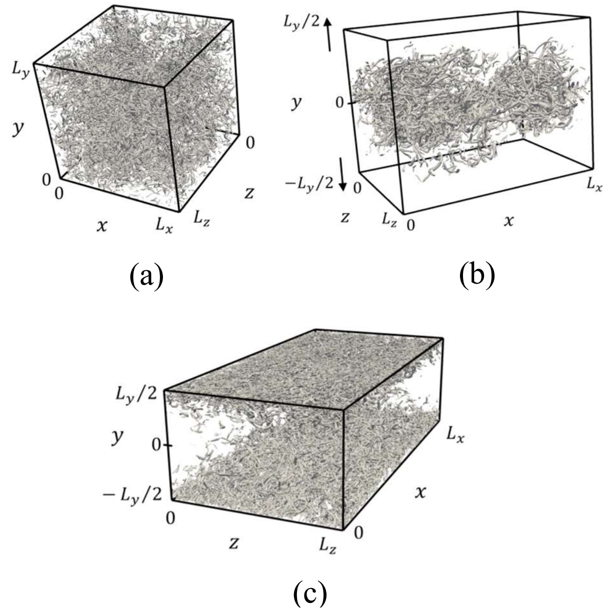

Figure 2. Typical instantaneous field of the second invariant of the velocity gradient tensor $Q = 0.02\max(Q)$ for (a) HIT120, (b) TML1300 and $Q = 0.005\max(Q)$ for (c) CH800.

initial vorticity thickness for TML. Such DNS data are preprocessed through filtering operation and mapped onto much coarser LES mesh to emulate LES fields using Gaussian filter kernel for the training process. The filter size Δ is set as ranges $\Delta/\eta = 1.6 - 86$. Here, η denotes Kolmogorov length scale in each flow field. In addition to those LES dataset, data augmentation is applied since the rotated input/output data is a completely unknown flow configuration for neural network models even though the data is physically identical to the original data, while the Galilean or translation invariants are naturally considered. The input/output quantities in each dataset are multiplied by the rotation matrix around an axis incrementing by $\pi/4$ to satisfy the rotational invariant discretely. 20% of the training data is used for validation and the model is saved when the minimum validation loss is reached.

The GNN-based SGS model is additionally tested in stoichiometric hydrogen-air turbulent premixed combustion fields. Conventionally, SGS stress models developed for non-reacting incompressible flows have been applied to variable-density reacting flows with assumed validity. Here, two turbulent combustion configurations are tested. One is statistically planar flames where the flames freely propagate in homogeneous isotropic turbulence (PF in Table 1) (Shim *et al.*, 2011), and the other is turbulent V-flame (VF in Table 1) (Minamoto *et al.*, 2011), where turbulent V-flame anchored by the presence of a hot rod produces shear layers with large shear stress. For these two cases, the Reynolds number is defined based on the inlet Taylor microscale. Both combustion DNS data are also preprocessed in the same way as the incompressible data, and the filter size is set as $\Delta = 0.25\delta_{th}$, where δ_{th} is the flame thermal thickness.

MODEL ASSESSMENT

The prediction performance of the GNN-based SGS stress model is assessed in a priori manner for incompressible turbulent flow configurations. Figure 3 shows joint probability density functions of the target values created from the filtered DNS and predicted SGS stress tensor components $\tau_{11}, \tau_{12}, \tau_{13}$. The predicted values by the GNN-based model show positive correlations with the target values, although the relatively

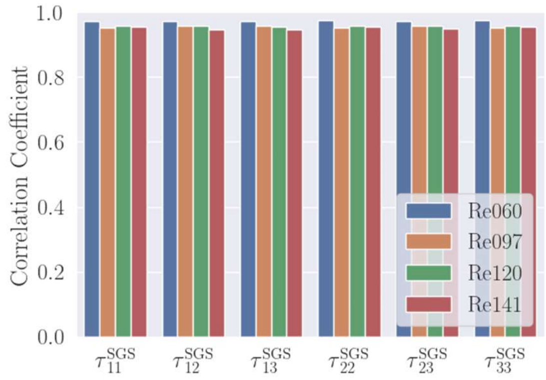

Figure 4. Correlation coefficients for each stress tensor component of HIT.

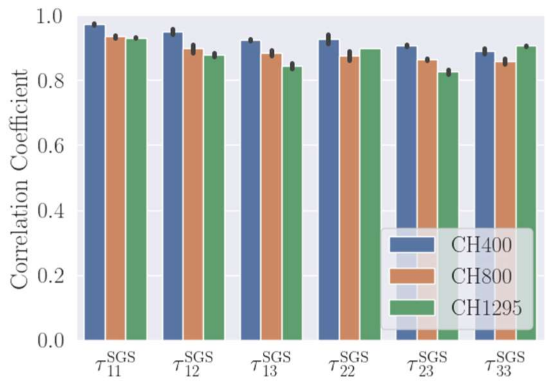

Figure 5. Correlation coefficients for each stress tensor component of CH.

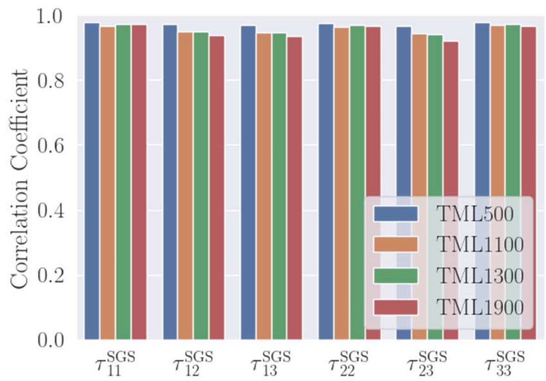

Figure 6. Correlation coefficients for each stress tensor component of TML.

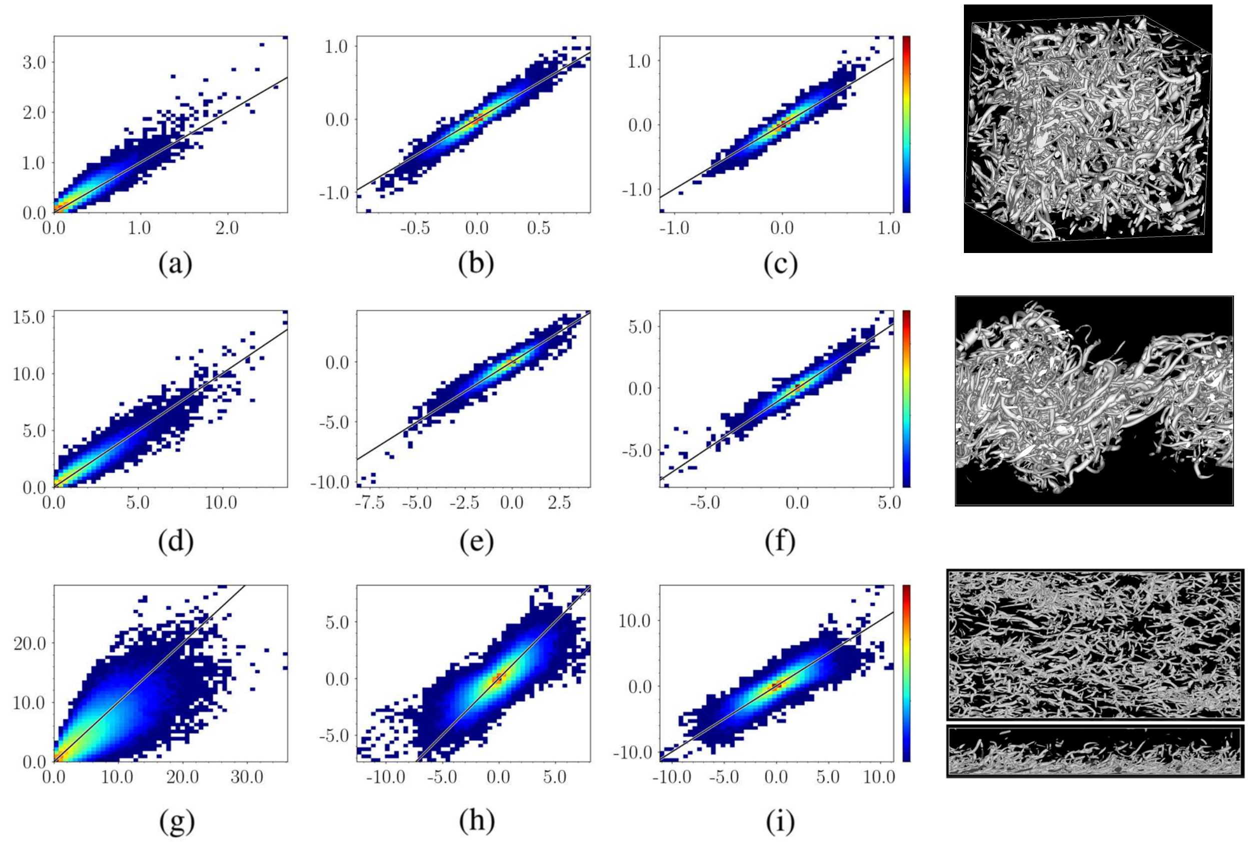

Figure 3. Joint probability density functions of the target (horizontal axis) and predicted (vertical axis) values. The predictions are shown for τ_{11} (a), (d), (g), τ_{12} (b), (e), (h), and τ_{13} (c), (f), (i), for HIT (a)-(c), TML (d)-(f), and CH (g)-(i). The color is in a logarithmic scale.

large variation is observed in turbulent channel flows. The correlation coefficients for each SGS stress tensor component of all the test cases considered are shown in Figure 4-6. In fact, the correlation coefficient for HIT ranges 0.92-0.93, for CH 0.84-0.93 and for TML 0.91-0.97, and the value averaged over all six stress components is well over 0.8 in each test flow condition. The root mean squared error for HIT and TML is approximately 0.2 and for CH approximately 0.6 at most in each stress tensor component.

Furthermore, the GNN-based SGS stress model is tested in turbulent combustion fields. The output of the model is conditioned by the reaction progress variable $\tilde{c}_T$ based on the mixture GS temperature defined as $\tilde{c}_T = (\tilde{T} - T_u)/(T_b - T_u)$, where T_u is the preheated temperature of the reactant and T_b is the burnt temperature. Figure 7 shows the joint probability density functions of the target and predicted values for the reaction zones ($0.2 \leq \tilde{c}_T < 0.4$). While the presence of significant density fluctuations inside the reaction zones due to combustion exists, the overall trends exhibited in the PDF are close to those observed in the result of the testing in incompressible turbulent flows. The correlation coefficient ranges between 0.74-0.96 for the planar flame and 0.92-0.97 for the V-flame for all six stress tensor components inside the reaction zones. In the unburnt side, the correlation coefficients range between 0.93-0.97 and in the burnt side they range 0.76-0.97 for both combustion cases. The prediction accuracy is slightly lower in diagonal components of the SGS stress tensor inside the reaction zones, and it can be found that overprediction of the stress in diagonal components is much less for V-flame than planar flame. This is because there exist large density fluctuations caused by combustion inside the reaction zones while the model is trained only on incompressible flows.

CONCLUSIONS

In the present study, the ML-based SGS stress model is developed in a way that resolves the potential limitations appearing in the current ML-based SGS stress models or their practical applications in LES. The training dataset includes fundamental incompressible turbulent flows; homogeneous isotropic turbulence, turbulent channel flow and temporally developing turbulent mixing layer with different Reynolds numbers. The result of a priori testing on incompressible turbulent flows showed that the GNN-based model yields reasonable prediction performance, regardless of flow configurations and Reynolds numbers. In addition, the model is assessed in turbulent combustion fields, which showed relatively strong positive correlations overall between the filtered DNS and the output of the model inside the reaction zones for both planar flames and V-flame. The model overpredicted the SGS stress in the diagonal components due to large density fluctuations since the model does not consider dilation. Outside the reaction zones, where density fluctuation is smaller, the model performance is satisfying overall as well, although the prediction of the SGS stress model in those regions is less important than the reaction zones in turbulent combustion LES. Future work includes considering

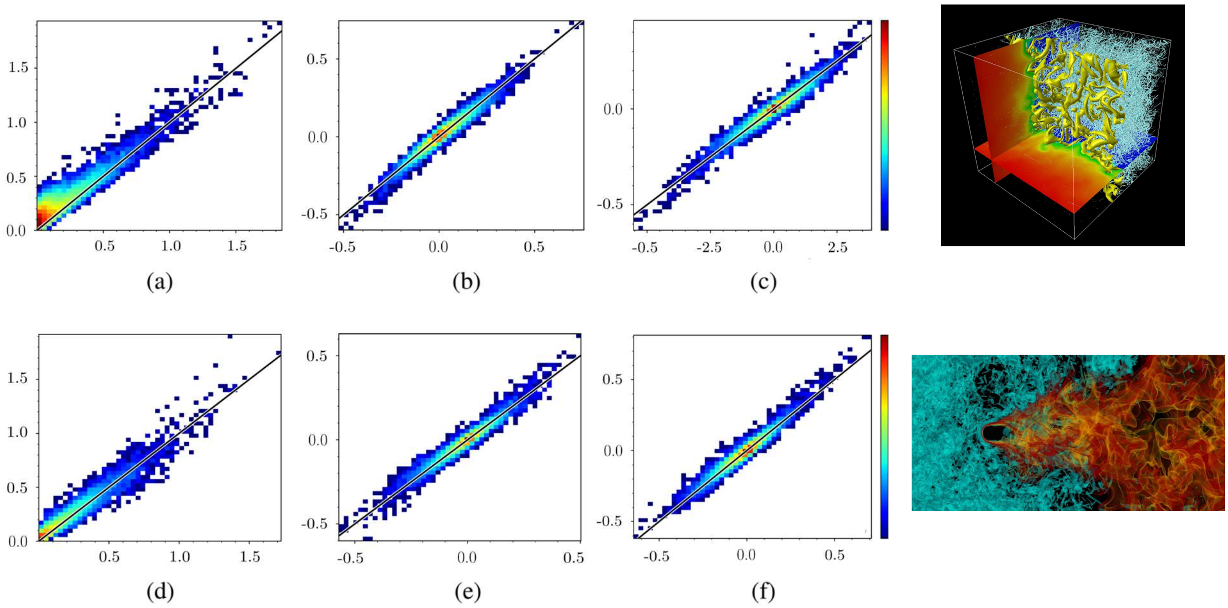

Figure 7. Joint probability density functions of the target (horizontal axis) and predicted (vertical axis) values of τ_{11}, τ_{12} and τ_{13} for planar (a)-(c) and V-flame (d)-(f)in the reaction zones. The axis values are divided by 10^2 (a)-(c) and by 10^3 (d)-(f). Both axes are in $\mathrm{kg/m/s^2}$. The color is in a logarithmic scale.

compressible flows in the training dataset in order to improve the performance inside the reaction zones.

REFERENCES

Abekawa, A., Minamoto, Y., Osawa, K., Shimamoto, H. and Tanahashi, M., "Exploration of robust machine learning strategy for subgrid scale stress modeling", *Phys. Fluid* 35, 015162 (2023).

Bardina, J., "Improved turbulence models based on Large Eddy simulation of homogeneous, incompressible, turbulent flows", Ph.D. thesis, Stanford University, Stanford, CA (1983).

Clark, R., "Evaluation of sub-grid scalar models using an accurately simulated turbulent flow". *J. Fluid Mech*., 91 (1979), 1-16.

Fey, M., Lenssen, J. E., Weichert, F. and Müller, H., "SplineCNN: Fast geometric deep learning with continuous B-spline kernels", *Proc. IEEE CVPR* (2018), pp.869-877.

Gamahara, M. and Hattori, Y., "Searching for turbulence models by artificial neural network", *Phys. Rev. Fluids* 2, 054604 (2017).

Itoh, T., Naka, Y., Minamoto, Y., Shimura, M. and Tanahashi, M., "Large-scale clustering of coherent fine-scale eddies in a turbulent mixing layer", *Int. J. Heat Fluid Flow* 72, 100-108 (2018).

Kang, S. J., Tanahashi, M. and Miyauchi, T., "Dynamics of fine scale eddy clusters in turbulent channel flows", *J. Turbulence* 18(52) (2007), pp.1-19.

Krizhevsky, A., Sutskever, I., and Hinton, G., "ImageNet classification with deep convolutional neural networks", in *Advances in Neural Information Processing System 25* (2012), pp. 1097-1105.

Liu, B., Yu, H., Huang, H., Liu, N., and Lu, X., "Investigation of nonlocal data-driven methods for subgrid-scale stress modeling in large eddy simulation", *AIP Adv*., 12 (2022), 065129.

Minamoto, Y., Fukushima, N., Tanahashi, M., Miyauchi, T. Dunstan, T. D. and Swaminathan, N., "Effect of flow-geometry on turbulence-scalar interaction in premixed flames", *Phys. Fluid* 23, 125107 (2011).

Nikolaou, Z. M., Chrysostomou, C., Minamoto, Y., and Vervisch, L., "Evaluation of a neural network-based closure for the unresolved stresses in turbulent premixed V-flames", *Flow, Turbul. Combust.* 106 (2021), pp. 331-356.

Shim, Y., Tanaka, S., Tanahashi, M., and Miyauchi, T., "Local structure and fractal characteristics of H_2-air turbulent premixed flame", *Proc. Combust, Inst.* 33 (2011), pp.1455-1462.

Smagorinsky, J., "General circulation experiments with the primitive equations", *Monthly Weather Review*, 91, 99-164.

Sutskever, I., Vinyals, O., and Le, Q., V., "Sequence to sequence learning with neural networks", in *Advances in Neural Information Processing Systems 4* (2014), pp. 3104-3112.

Tanahashi, M., Miyauchi, T., and Ikeda, J., "Identification of coherent fine scale structure in turbulence", IUTAM symposium: Simulation and identification of organized structures in flows (1999), pp.131-140.

Tanahashi, M., Kang, S.J., Miyamoto, T., Shiokawa, S., and Miyauchi, T., "Scaling law of fine scale eddies in turbulent channel flows up to Reτ = 800", *Int. J. Heat Fluid Flow* 25 (2004), pp.331-340.

Tanahashi, M., Iwase, S., and Miyauchi, T., "Appearance and alignment with strain rate of coherent fine scale eddies in turbulent mixing layer", *J. Turbulence* 2 (2001), pp.1-17.

Vreman, B., Geurts, B., and Kuerten, H., "Large eddy simulation of the temporal mixing layer using the Clark model", *Theor. Comput. Fluid Dyn*., 8 (1996), 309-324.